



ARTICLE

## Novel Magnetically Interconnected Micro/Macroporous Structure of Monolithic Porous Carbon Adsorbent Derived from Sodium Alginate and Wasted Black Liquor and Its Adsorption Performance<sup>\*\*</sup>

Parichart Onsri<sup>1</sup>, Decha Dechtrirat<sup>2,3,4</sup>, Patcharakamon Nooeaid<sup>5</sup>, Apiluck Eiad-ua<sup>6</sup>, Pongsaton Amornpitoksuk<sup>1,7</sup>, Supanna Techasakul<sup>4</sup>, Ahmad Taufiq<sup>8</sup> and Laemthong Chuenchom<sup>1,7,\*</sup>

<sup>1</sup>Division of Physical Science, Faculty of Science, Prince of Songkla University, Songkhla, 90112, Thailand

<sup>2</sup>Department of Materials Science, Faculty of Science, Kasetsart University, Bangkok, 10900, Thailand

<sup>3</sup>Specialized Center of Rubber and Polymer Materials for Agriculture and Industry (RPM), Faculty of Science, Kasetsart University, Bangkok, 10900, Thailand

<sup>4</sup>Laboratory of Organic Synthesis, Chulabhorn Research Institute, Bangkok, 10210, Thailand

<sup>5</sup>Division of Polymer Materials, Faculty of Agricultural Product Innovation and Technology, Srinakharinwirot University, Nakhon Nayok, 26120, Thailand

<sup>6</sup>College of Nanotechnology, King Mongkut's Institute of Technology Ladkrabang, Bangkok, 10520, Thailand

<sup>7</sup>Center of Excellence for Innovation in Chemistry, Faculty of Science, Prince of Songkla University, Songkhla, 90112, Thailand

<sup>8</sup>Department of Physics, Faculty of Mathematics and Natural Sciences, Universitas Negeri Malang, Malang, 65145, Indonesia

\*Corresponding Author: Laemthong Chuenchom. Email: laemthong.c@psu.ac.th

Received: 14 August 2020 Accepted: 27 September 2020

### ABSTRACT

The novel and facile preparation of magnetically interconnected micro/macroporous structure of monolithic porous carbon adsorbent (MPCA) were designed and presented herein. The synthesis was achieved *via* conventional freeze-drying and pyrolysis processes. In this study, sodium alginate and wasted black liquor were employed as starting precursors. Sodium alginate acts as a template of materials, whereas black liquor, the wasted product from the paper industry with plentiful of lignin content and alkaline solution, played an essential role in the reinforcement and activation of porosity for the resulting materials. Moreover, both the precursors were well dissolved in Fe<sup>3+</sup> solution, providing a simple addition of a magnetic source in a one-pot synthesis. The interconnected micro/macroporous structures were generated through freeze-drying and, subsequently the pyrolysis process. The obtained cylindrical-shaped monolithic porous carbon adsorbent (MPCA-700) showed high mechanical stability, a high BET specific surface area (902 m<sup>2</sup>/g). Such aforementioned features were considered suitable to make the synthesized monolith as an adsorbent for the removal of heavy metal ions. The maximum adsorption capacity of MPCA-700 towards Pb<sup>2+</sup> ions was 76.34 mg/g at pH 5. The adsorption studies illustrated that adsorption kinetics and isotherm perfectly fitted with the pseudo-second-order kinetics model and Langmuir isotherm, respectively. This work presents a promising protocol to reduce the overall costs in the preparation of renewable adsorbents with good adsorption efficiency and regeneration.

\*\* This paper is an extended and revised article presented at the International Conference on Sustainable Energy and Green Technology 2019 (SEGT 2019) on 11–14 December 2019 in Bangkok, Thailand.



**KEYWORDS**

Hierarchical porous carbon monoliths; magnetic properties; adsorption; alginate; black liquor

**1 Introduction**

Since the industrial revolution, a third of the economic output has possibly come from manufacturing industries resulting in the economic system of either the developed countries or developing countries [1]. Among industry activities, proper waste management must be concerned [2].  $Pb^{2+}$  ions are one of the toxic heavy metals, which is released by various manufacturers such as the plating of metal, production of batteries, and electronic industries [3]. Its release causes environmental problems and affects the well-being of both humans and animals. Lead ions can possibly approach the human physique *via* inspiration, ingestion, and even skin contact. It may assemble in many organelles such as bones, brain, kidney, and muscles, severely damaging the body system [4].

In addition, the World Health Organization (WHO) assigns the maximum allowed limit of  $Pb^{2+}$  in potable water at as low as 0.05 ppm [5]. Therefore, the elimination of  $Pb^{2+}$  ions from the water stream is urgently needed.

Several techniques have been used to remove the  $Pb^{2+}$  ions from aqueous phase, including adsorption [6,7], precipitation [8], membrane filtration [9], reverse osmosis [10], solvent extraction [11], photochemical degradation [12], and bioremediation [13]. Among these techniques, adsorption is an economically feasible, effective technique for removing metal ions [14]. Porous carbon adsorbents with magnetic properties have conquered synthetic activated carbon because they can easily be separated from the water system by applying an external magnet [15], resulting in a reduction in time consumption.

Nevertheless, a well-distribution of magnetic iron particles in powdery porous carbons is difficult to control [16]. Therefore, part of non-magnetic particles could lead to secondary contamination [17]. To overcome this problem, the magnetic porous carbon materials in a monolithic form are more promising. Furthermore, the excellent monolithic porous carbon adsorbent (MPCA) should possess a hierarchical manner, consisting of several pore size ranges. The macroporous structure provides rapid mass transportation of adsorbate to active sites (mesoporous or microporous structures) of the adsorbent. The fabrication of MPCA with magnetic properties has been reported in a few publications. Then, the study of the preparation of MPCA with magnetic properties and interconnected micro/macroporous structure is desirable.

Sodium alginate (NaAlg) is a biopolymer extracted from brown marine algae [18]. Several publications reported that NaAlg could be fabricated in sponge with macroporous structure *via* the freeze-drying process [19]. Although sodium alginate sponges are famous in engineering tissue, only a few reports used them as carbon-based materials in monolithic form due to their poor mechanical stabilities. Then, the improvement of mechanical stabilities in NaAlg is challenging. Herein, NaAlg was then selected as a macroporous template. Moreover, the solubility of NaAlg makes it easy to be mixed with other additives.

In paper manufacturing, there are plentiful amounts of wasted black liquor (WBL) residue from the Kraft pulping process [20]. Generally, the pretreatment and purification processes are required to extract lignin contents or other substrates from WBL, which takes extra costs and is time-consuming [21]. Therefore, adding the value of waste materials with simple steps has become a challenge for practical applications. WBL is mainly comprised of lignin contents and alkaline additives such as NaOH and KOH. The unique chemical structure of lignin could improve the robustness of carbon materials during the calcination process [22]. Also, the presence of alkalis could enhance the porosity and surface area of carbon materials because they act as activating agents [23]. Since WBL is soluble in aqueous solution, this results in excellent compatibility between WBL and NaAlg.

Therefore, in this work, we show that the novel magnetically interconnected micro/macroporous structure carbon monoliths can easily be fabricated by simple mixing of NaAlg and WBL in  $\text{Fe}^{3+}$  solution. The purposed synthesis protocol only undergoes 2 steps; the first process is a freeze-drying process to generate the macroporous sponge with the assistance of NaAlg, and the latter pyrolysis converts macroporous sponge into interconnected micro/macroporous structure of monolithic porous carbon adsorbents (MPCA). The carbon monoliths prepared using the protocol in this research seem to be promising and renewable adsorbents. This is because the use of such carbon monoliths as adsorbents can reduce the overall costs of adsorption and regeneration due to their facile operation of the monolithic adsorbent with high stability. Also, the prepared carbon monolith showed good magnetic separation and adsorption properties towards lead ions with good mechanical stability and facile regeneration process.

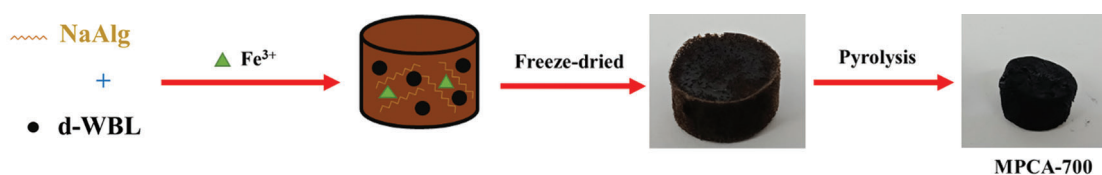
## 2 Materials and Methods

### 2.1 Chemicals and Reagents

All of the chemicals were analytical grade. Sodium alginate was purchased from Sigma-Aldrich. Hydrochloric (HCl, 37%) and sodium chloride (NaOH, 99.0%) were purchased from J.T. Baker. Ferric chloride hexahydrate ( $\text{FeCl}_3 \cdot 6\text{H}_2\text{O}$ , 99.0%) was purchased from Loba Chemie. Lead (II) chloride ( $\text{PbCl}_2$ ) was purchased from Fluka Chemika. Black liquor obtained from the Kraft pulping process of the Siam Cement Pcl (Thailand) was used without any purifications. Deionized water (DI) was used for all experiments.

### 2.2 Preparation of Magnetically Interconnected Micro/Macroporous Structure of MPCA

Firstly, wasted black liquor (WBL), a viscous liquid, was dried at  $105^\circ\text{C}$  in an oven. The obtained dried-wasted black liquor was denoted as d-WBL and kept in the desiccator to prevent the moisture before being further used. Next, 4.0 g of d-WBL and 4.0 g of NaAlg were dissolved together in 50 ml of iron solution (prepared by 0.5 g of  $\text{FeCl}_3 \cdot 6\text{H}_2\text{O}$  in 50 ml of DI water). The dark-brown viscous mixture was cast into a cylindrical mold (24-well plate) and stored at  $-4^\circ\text{C}$  in the refrigerator overnight, and the sample was freeze-dried at  $-80^\circ\text{C}$ . Then, the freeze-dried porous sponges were pyrolyzed under  $\text{N}_2$  gas at a heating rate of  $1^\circ\text{C}/\text{min}$  for 1 h at the desired temperature. The pyrolyzed products were rinsed several times with hot DI water until a neutral pH was reached to remove excess salt products and ashes. The final products were denoted as MPCA-T, where T represents the pyrolysis temperature. The synthesis procedure of the magnetically interconnected micro/macroporous structure of MPCA is shown in [Sch. 1](#).



**Scheme 1:** Schematic illustration of the preparation of magnetically interconnected micro/macroporous structure of MPCA-700

### 2.3 Characterization Studies

The thermal degradation of the freeze-dried porous sponges was investigated using a Thermogravimetric Analyzer instrument (TGA, Perkin Elmer, TGA8000). The condition of the experiment was operated under the  $\text{N}_2$  atmosphere in the range of  $50^\circ\text{C}$ – $1000^\circ\text{C}$  of temperature with  $5^\circ\text{C}/\text{min}$  of heating rate. The mechanical properties of the synthesized materials were evaluated in compression mode with a universal testing machine (Instron 5966, USA).

The surface morphology and elemental analysis of MPCA-700 were observed and determined using a Field Emission Scanning Electron Microscope (FESEM, FEI, Apreo) equipped with Energy-dispersive X-ray spectroscopy (EDS). Porous analysis of MPCA-700 was carried out by nitrogen sorption measurements at 77 K using the Surface Area and Porosity Analyzer (Micromeritics, ASAP2460), and the sample was degassed at 200°C for 900 min prior to the measurements. The specific surface area and pore size distribution were examined by Brunauer-Emmett-Teller (BET) and Density Functional Theories (DFT), respectively.

Phase identifications of crystalline and non-crystalline on MPCA-700 were collected on an X-Ray Diffractometer (XRD, Philips, X'Pert MPD) with Cu K $\alpha$  radiation source ( $\lambda = 0.154$  nm). The magnetization value of MPCA-700 was assessed by a vibrating sample magnetometer (VSM, Lakeshore) at 298 K. Chemical compositions and chemical bonding of materials were identified using X-ray photoelectron spectroscopy technique (XPS, Kratos Analytical Ltd., AXIS Ultra DLD). Surface functional groups of MPCA-700 were obtained from Fourier-transform infrared spectroscopy analysis (FTIR, Bruker, VERTEX70).

#### **2.4 Stability of Magnetically Interconnected Micro/Macroporous Structure of Monolithic Porous Carbon Adsorbent Monolith against Acid Leaching**

The magnetic stabilities of MPCA-700 were investigated by using 0.03 g of MPCA-700 in 20 mL of 0.01 M NaCl solution set in a shaker incubator (Model TOL09-FTSH-01, SCIFINETECH), with 200 rpm at room temperature (RT) ( $30 \pm 2^\circ\text{C}$ ) for 24 h. The initial pH of NaCl was adjusted in the range of 2–7 using 0.1 M NaOH and 0.1 M HCl. The total concentration of Fe ions, which was leached from the monolith, was examined with an Inductively Coupled Plasma-Optical Emission Spectrometry (ICP-OES, PerkinElmer, Avio500).

#### **2.5 Batch Adsorption Studies**

Batch adsorption studies were performed for evaluation of the adsorption capacity of MPCA-700 towards Pb<sup>2+</sup> ions. 0.03 g of MPCA-700 was used as a selected adsorbent in all experiments. The effect of initial pH on adsorption ability was carried out in 100 mg/L of Pb<sup>2+</sup> solution ranging from pH 3 to 5 adjusted by 0.1 M HCl and 0.1 M NaOH for 24 h. After the adsorption equilibrium was reached, MPCA-700 was separated from the system by using an external magnet. The concentrations of Pb<sup>2+</sup> ions in solution before and after adsorption were diagnosed using the calibration method with ICP-OES.

For kinetic studies, MPCA-700 was shaken in 200 mL of 100 ppm Pb<sup>2+</sup> solution (pH 5) set in a shaker incubator, with 150 rpm at RT. Then, 0.5 mL of adsorbate solutions were withdrawn from the solution at desired time intervals and then subject to measurements of concentrations. The adsorption capacity at pre-determined time intervals,  $q_t$  (mg/g) of MPCA-700 toward Pb<sup>2+</sup> ions was calculated using Eq. (1):

$$q_t = \frac{V (C_0 - C_t)}{m} \quad (1)$$

where  $C_0$  and  $C_t$  are the initial concentration and concentration at pre-determined time intervals ( $t$ ) of Pb<sup>2+</sup> ions (mg/L), respectively.  $V$  is Pb<sup>2+</sup> solution volume (L), and  $m$  is MPCA-700 weight (g).

For adsorption isotherm studies at equilibrium, experiment conditions were similarly performed for kinetic studies. Initial concentrations of 100 ml of Pb<sup>2+</sup> ions were adjusted in the range of 100–500 mg/L (pH 5) for 24 h. The equilibrium adsorption capacity ( $q_e$ , mg/g) of Pb<sup>2+</sup> on MPCA-700 was calculated using Eq. (2):

$$q_e = \frac{V (C_0 - C_e)}{m} \quad (2)$$

where  $C_e$  is the equilibrium concentrations of  $Pb^{2+}$  (mg/L).

### 2.6 Desorption Studies and Recyclability

The recyclability of MPCA-700 was studied with 25 ml of 25 ppm  $Pb^{2+}$  ions for 24 h at RT. After the adsorption process, the simple desorption of  $Pb^{2+}$  ions from the adsorbed MPCA-700 was carried out by immersing and shaking the monolith in 25 mL of 0.001 M  $HNO_3$  (pH 3), for 24 h. Then, MPCA-700 was washed with DI water and dried in an oven at 100°C overnight. The dried sample was applied in the next adsorption-desorption cycles for 5 consecutive runs with the same volume and concentration for both adsorption and desorption as in the first cycle. The released amount of  $Pb^{2+}$  ions in each cycle was used to calculate %desorption according to Eq. (3):

$$\%desorption = \frac{\text{released concentration of } Pb^{2+} \text{ from MPCA-700 in each cycle}}{\text{amount of } Pb^{2+} \text{ ions adsorbed in MPCA-700 in each cycle}} \times 100 \quad (3)$$

## 3 Results and Discussion

### 3.1 Characterizations of Magnetically Interconnected Micro/Macroporous Structure of MPCA

The first step of the preparation process of MPCA-T was based on the freeze-drying process. The principle of using the freeze-drying was to generate ice crystals, which acted as a template for macropores. By considering the fact that all the starting compositions in our system (WBL, NaAlg,  $Fe^{3+}$  ions) were well soluble in water, the homogeneous dark-brown viscous mixture was then obtained. However, it was found that this mixture always stayed fluid and never became completely solidified even after 2 h under ambient conditions (no wet gel obtained). This behavior indicated that the starting chemicals did not completely crosslink at RT. For this reason, the freeze-drying was then performed to well distribute the ice crystals throughout the monolith, as well as to prevent the macropores from being collapsed. The hot-drying process around 100°C was also attempted, but the sample became flat, and only a flat sheet at the bottom of the mold could be obtained. This result stresses the importance of the freeze-drying to keep the monolithic shape and pore texture intact.

After the freeze-drying, a stable freeze-dried porous sponge could be obtained. Since the freeze-dried sponge was not completely cross-linked, the sponge became wet and redissolved when exposed to the liquid water or ethanol. These observations found in this step provide evidence that, in contrast to simple hot-drying or solvent exchange processes in the conventional synthesis of resorcinol-formaldehyde-based porous carbon monoliths [24,25]. The cross-linking of the obtained MPCA was achieved upon the pyrolysis, resulting in a rigid carbon monolith.

The temperature condition of the pyrolysis process had a direct influence on the mechanical stability of the MPCA. MPCA-800 was in an irregular shape and fragile due to the collapse of the porous structure upon high-temperature pyrolysis. In contrast, the primitive shape of MPCA-700 could be retained (Sch. 1) and exhibited strong mechanical stability (Fig. 1A). The plot of compressive stress as a function of strain on MPCA-700 was more than six times higher than freeze-dried porous sponges at 20% strain because the heating temperature could generate the condensed structure and the crosslinking of carbon precursors. The smooth curve of the freeze-dried porous sponge represented the homogeneity of macropore sizes after the freeze-drying process. However, after the pyrolysis process, the roughness of the MPCA-700 curve was observed, implying the different sizes of porous structures. The thermal degradation of the freeze-dried porous sponge was investigated with TGA/DTG, and the result is shown in Fig. 1B. There are two main degradation steps; the first step was the removal of humidity on the freeze-dried porous

sponge at a temperature lower than 150°C and the second step occurred during 150°C–800°C related to the degradation of NaAlg and WBL precursor [19]. The sharp peak in the DTG profile at the first degradation step resulted from the loss of a high amount of hydroxyl groups in the NaAlg and lignin contents. Also, the activating agents such as NaOH and KOH in WBL provide a hygroscopic phenomenon, which is sensitive to trapping the humidity.

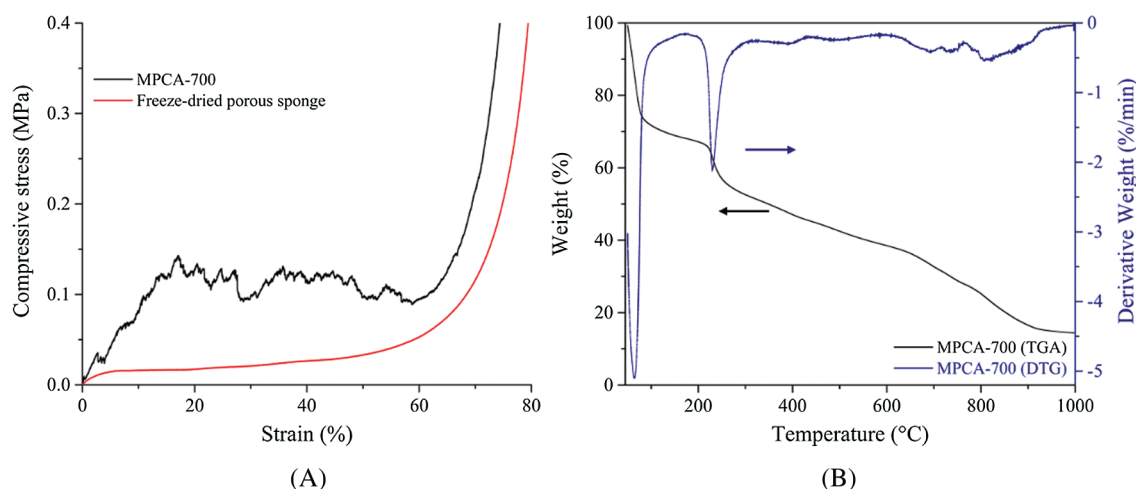


**Figure 1:** (A) The plot of compressive stress as a function of strain on MPCA-700 compared with the freeze-dried porous sponge and (B) TGA/DTG profiles of the freeze-dried porous sponge

The photograph of the prepared materials before and after pyrolysis at 700°C is shown in Fig. 2A. The shrinkage of the porous carbon materials upon the pyrolysis process was commonly observed, in agreement with weight loss from the TGA results. However, the prepared materials in this study had only 30% volume shrinkage; as a result of the benefit of the lignin-containing in WBL. Previous studies have confirmed that lignin-containing precursors could stand high temperatures with low weight loss due to its condensed aromatic units, which was attractive to be used as a precursor to synthesize carbon fibers [26].

The pore morphology of MPCA-700 was studied using the FESEM technique, and the FESEM results are shown in Figs. 2B and 2C. The pore texture of MPCA-700 comprised large macropores interconnected with small macropores associated with the roughness of the compressive stress-strain curve in Fig. 1A. The distribution of elements on the prepared sample was evaluated by EDS-mapping shown in Fig. 2D. The results showed that iron particles were regularly dispersed throughout the sample. The good distribution of iron particles resulted from the excellent compatibility between NaAlg, WBL, and iron solution.

Pore textures of MPCA-700 were studied by N<sub>2</sub> sorption experiments. The result of N<sub>2</sub> adsorption-desorption isotherm of MPCA-700 in Fig. 3A revealed the type I isotherm, classified as micropores (size < 2 nm). The inset figure displays the pore size distribution of MPCA-700 calculated by the DFT method. The sharp maximum pore size distribution is located at 1.20 nm, revealing the sample contained dominant pore sizes of micropores. However, the isotherm shows a hysteresis loop, indicating that the sample might contain a slight degree of mesopore fractions. The high BET specific surface area of 902 m<sup>2</sup>/g of MPCA-700 could be generated by NaOH/KOH in WBL, and Fe<sup>3+</sup> ions acted as activating agents at high temperature [27].

The elemental and chemical composition of MPCA-700 was also analyzed by using the XPS technique. From Fig. 3B, the wide scan provided the details of the elemental composition composed of C 1s, O 1s, Fe 2p, Si 2p, Na 1s, Ca 2p, and K 2p, and the values of chemical compositions are exhibited in Tab. 1. The iron

content is as high as 25.98%, indicating the excellent diffusion of  $\text{Fe}^{3+}$  ions in the mixing solution. The presence of inorganic elements, for instance, Si, Ca, and K was undoubtedly from WBL. The relatively high content of oxygen was, as a result, high oxygen in NaAl precursor.

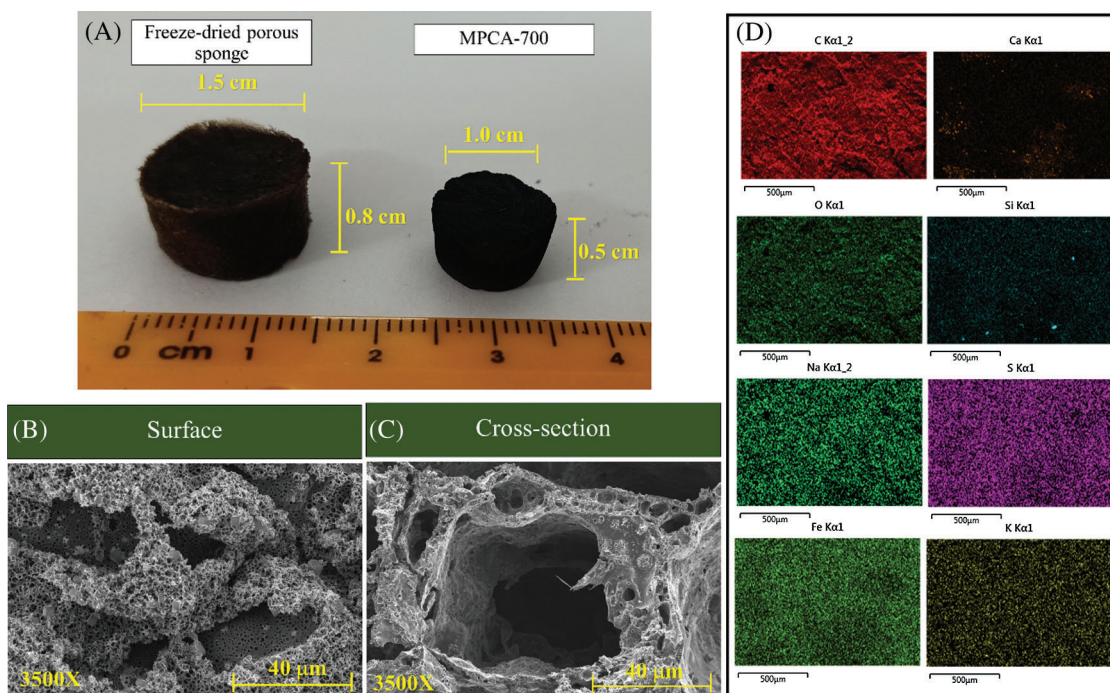


**Figure 2:** (A) A digital photo of the freeze-dried porous sponge and MPCA-700, (B) FESEM image of the surface of MPCA-700 at a magnification of 3500 $\times$ , (C) FESEM image of the cross-section of MPCA-700 at a magnification of 3500 $\times$ , and (D) EDS-mapping of MPCA-700

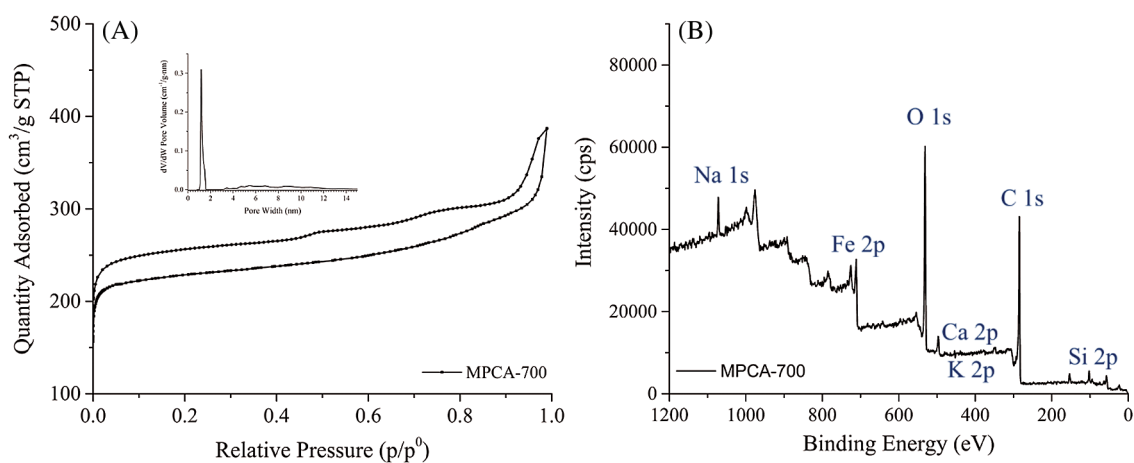


**Figure 3:**  $\text{N}_2$  sorption isotherm of MPCA-700 and the inset figure exhibited the pore size distribution of MPCA-700 and B: wide scan XPS spectrum of MPCA-700

**Table 1:** The detail of the chemical compositions of MPCA-700

Sample	Chemical compositions (%)						
	C 1s	O 1s	Fe 2p	Si 2p	Na 1s	Ca 2p	K 2p
MPCA-700	43.30	21.31	25.98	4.81	2.87	1.42	0.32

Phase identification of MPCA-700 was studied by using the XRD technique. XRD pattern in Fig. 4A reveals 3 sharp diffraction peaks as a result of the existence of the metallic iron phase (ICDD file no. 00-006-0696) at  $2\theta$  values of  $44.67^\circ$ ,  $65.02^\circ$ , and  $82.33^\circ$  regarding (110), (200) and (211) facets, respectively. Besides, the broad peak at  $2\theta$  values of  $26.2^\circ$  and  $43^\circ$  associated with (002) and (100) planes, respectively, exhibited the existence of turbostratic carbon. The metallic iron phase contained in MPCA-700 made this material possesses a saturation magnetization of  $8.8 \text{ emu/g}$  (Fig. 4B), enough for easy separation from the aqueous phase using an external magnet (inset in Fig. 4B). Moreover, the inset picture displays that the high magnetic stability of MPCA-700 could be retained, as confirmed by the strong attraction by an external magnet even after the complete adsorption over 24 h.

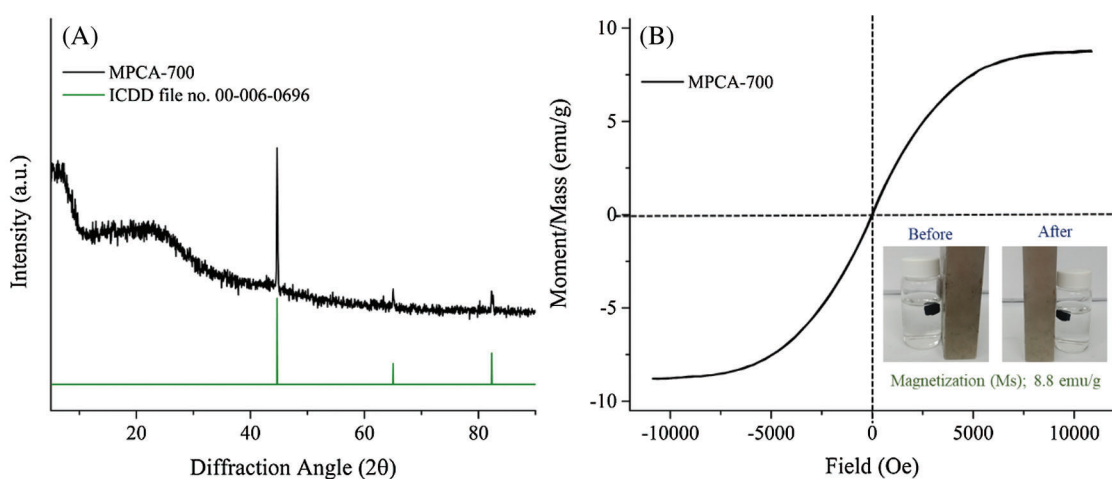


**Figure 4:** (A) XRD pattern, and (B) Magnetic hysteresis loops of MPCA-700, inset in B shows the magnetic stability of the sample before and after adsorption, being attracted using a magnet

Although the prepared MPCA-700 in our study had an iron content of 25.98% from XPS analysis, its saturated magnetization was found to be lower than those of the others in Tab. 3. In general, there are several factors affecting the magnetization, such as the phase of iron species, number of iron particles, particle size of the iron particles, and the matrix compositions, as well as how the measurements are performed. The phase of iron species could be used to explain why MPCA-700 had a low value in the saturated magnetization, even though it contained high iron content. According to Tab. 3, all the adsorbents in other works containing the magnetite ( $\text{Fe}_3\text{O}_4$ ) phase showed higher saturated magnetization compared to the ferrite ( $\text{Fe}^0$ ) phase in our study [27–31]. However, the preparation method in this study is a simple one-pot synthesis without the preparation of preformed  $\text{Fe}_3\text{O}_4$ , significantly reducing the time consumption and chemicals.

### 3.2 Batch Adsorption Studies: Effect of pH, Kinetics, and Adsorption Capacity

The high magnetic stability of iron-containing-based magnetic porous carbons against a change in pH variation is necessary. This is because when the iron containing-based magnetic adsorbents are applied in

practical adsorption conditions, the secondary contamination from iron leaching should be avoided. Fig. 5A reveals that iron species in MPCA-700 can be leached under the strong acid condition at pH 2 with 32.38 mg/L. However, the prepared adsorbent has high magnetic stability in the range of pH 3–7. In this study, the influence of initial pH on equilibrium adsorption capacity towards  $\text{Pb}^{2+}$  was operated in the range pH 3–5 because the lead solution can be precipitated into lead hydroxides under alkaline solution ( $\text{pH} \geq 6$ ) [32]. The result indicates that the highest adsorption performance of MPCA-700 towards  $\text{Pb}^{2+}$  ions was achieved at pH 5, with an adsorption capacity of 62.71 mg/g. This behavior could be explained by the surface charge of MPCA-700 measured by zeta potential (Fig. 5B). It is clear that the surface charge of MPCA-700 at pH 5 is the least positive charge over the range of adsorption experiments, which provides more attractive interactions between adsorbent surfaces and  $\text{Pb}^{2+}$  ions. Therefore, ionic interactions are one of the dominant factors associating to the removal of  $\text{Pb}^{2+}$  by MPCA-700. Besides the ionic interactions, adsorption affinities can possibly occur through other interactions, such as pore-filling effect, and ion exchange. The pore-filling effect is typically present for adsorbents with high surface area and pore volume [33].

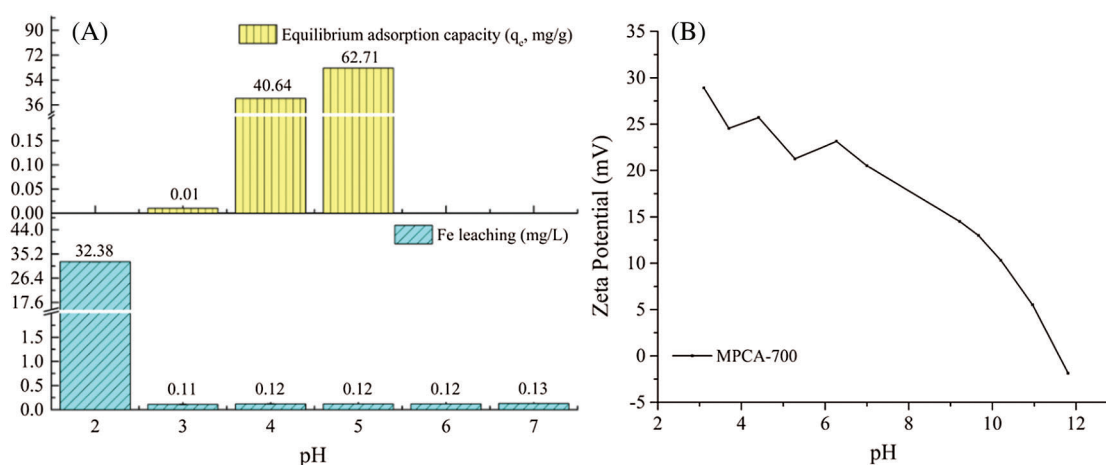


**Figure 5:** (A) The stabilities against acid conditions and the influence of initial pH on adsorption capacity, and (B) Zeta potential plot of MPCA-700

The effect of contact time on  $\text{Pb}^{2+}$  ions adsorption ability by MPCA-700 was studied, and the results are shown in Fig. 6A. It is clearly seen that at the initial stage, the adsorption of MPCA-700 was significantly rapid due to unoccupied adsorption sites and reached the adsorption equilibrium in 250 min. To assess the adsorption kinetics, the adsorption data were conformed with the models of non-linear equations of pseudo-first-order and pseudo-second-order, as displayed in Tab. 2. The assumption of the pseudo-first-order model involves the adsorption rate of the solute related to the saturation concentration and the sorbent content changes to the exposure time. For the pseudo-second-order kinetic model, it represents that the chemical adsorption slows down the reaction speed and controls the adsorption processes [34]. In this study, the determination coefficient ( $R^2$ ) of 0.9993 suggested that the adsorption kinetics of MPCA-700 fits the pseudo-second-order model, indicating that the adsorption occurs on the localized sites without interactions between adsorbates [34]. Moreover,  $q_e$  values from experimental and calculated are indistinguishable (145 and 147.06 mg/g, respectively). In general, the powdery adsorbents have shown fast adsorption kinetics due to the abundant open pores on the small particles in micrometer-down to nanometer-sizes, allowing the rapid adsorption contact with the adsorbate molecules [35]. Notably, although MPCA-700 is in a monolith shape, the relatively fast kinetic rate ( $k = 3.07 \times 10^{-4} \text{ g mg}^{-1} \text{ min}^{-1}$ ) was achieved, indicating that the interconnected macroporous structures provided the rapid mass

transportation of  $\text{Pb}^{2+}$  ions into the adsorptive sites. Interestingly, the adsorption rate of MPCA-700 is equally or comparatively as high as those of magnetically powdery porous carbons in other works (Tab. 3).

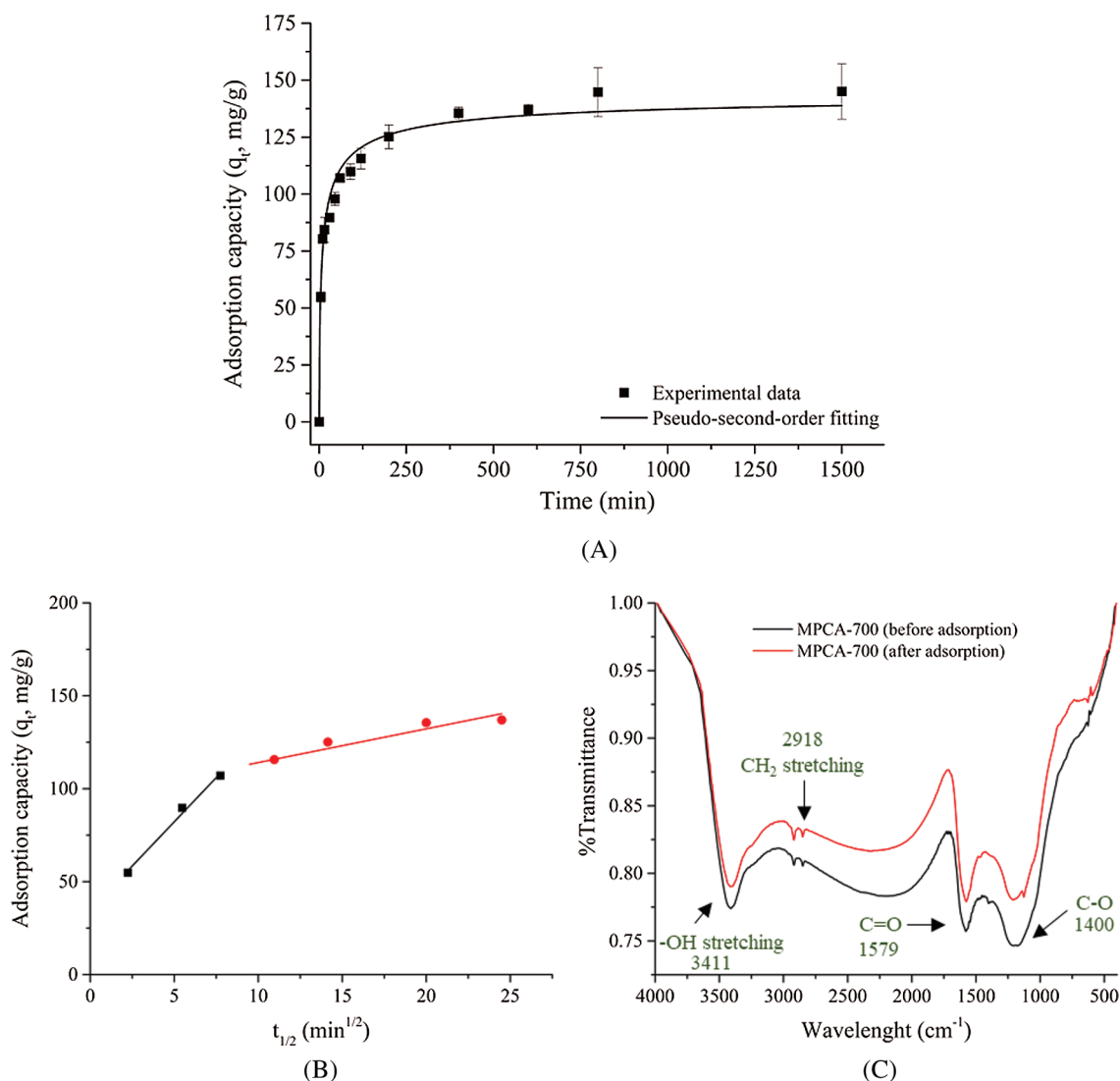


**Figure 6:** (A) Effect of contact time on  $\text{Pb}^{2+}$  ions adsorption by MPCA-700, (B) Two slopes of the intraparticle diffusion plot of MPCA-700 for  $\text{Pb}^{2+}$  ions removal, and (C) FT-IR spectra of MPCA-700 before and after adsorption

**Table 2:** Fitted parameters in adsorption studies of MPCA-700

Models and Parameters		$\text{Pb}^{2+}$		
Adsorption kinetics				
Pseudo first order	$q_{e(\text{cal})}$ (mg/g)	$q_{e(\text{exp})}$ (mg/g)	$K$ ( $\text{min}^{-1}$ )	$R^2$
	59.36	145	$6.5 \times 10^{-4}$	0.8814
Pseudo second order	$q_{e(\text{cal})}$ (mg/g)	$q_{e(\text{exp})}$ (mg/g)	$K$ ( $\text{g mg}^{-1} \text{min}^{-1}$ )	$R^2$
	147.06	145	$3.07 \times 10^{-4}$	0.9993

Models and Parameters		Pb <sup>2+</sup>		
Intra-particle diffusion		$k_{id}$ (mg g <sup>-1</sup> min <sup>-1</sup> )	X	R <sup>2</sup>
	at 0–60 min	9.567	34.54	0.9920
	at 120–800 min	1.545	101.35	0.9486
Adsorption isotherm				
Langmuir	$q_m$ (mg/g)	$k_L$ (L/mg)		R <sup>2</sup>
	76.34	0.22		0.9997
Freundlich	$k_F$	1/n		R <sup>2</sup>
	47.33	0.0815		0.9348

The intra-particle diffusion model was used to study the adsorption mechanisms in detail. Fig. 6B reveals the plot between adsorption capacity at different periods ( $q_t$ , mg/g) and  $t_{1/2}$  (min<sup>1/2</sup>). The two slopes of the linear line were seen, indicating two physical processes controlled the adsorption rate. At the time of 0–60 min, there was a high value of  $k_{id} = 9.567$  mg g<sup>-1</sup> min<sup>-1</sup>, implying the process of rapid film adsorption. The following process occurred during 120–800 min, involving the process of the intra-particle diffusion with the slow  $k_{id}$  of 1.545 mg g<sup>-1</sup> min<sup>-1</sup>, which is the rate-limiting step.

FT-IR spectra of MPCA-700 before and after the adsorption experiment in Fig. 7C could further explain the interactions between adsorbent and adsorbate. Several oxygen-related functional groups promote a possibility to share or exchange electrons with Pb<sup>2+</sup> ions, resulting in a slight shift of wavenumbers of functional groups, including –OH stretching, CH<sub>2</sub> stretching, C=O, and C–O after adsorption experiments [3].

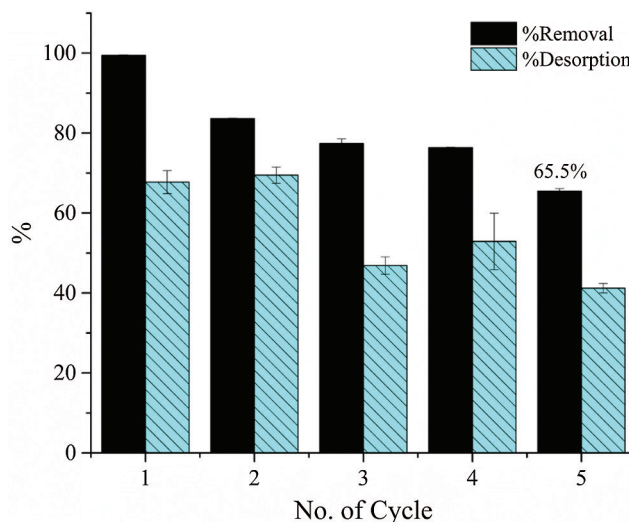


**Figure 7:** Plot showing %removal and %desorption of Pb<sup>2+</sup> ions by MPCA-700 in each cycle (initial concentration; 25 ppm, volume; 25 mL and time; 24 h)

To investigate the equilibrium adsorption isotherm, the experiments were performed similarly to kinetics study by varies the initial concentrations of 100 ml Pb<sup>2+</sup> ions in the range of 100–500 mg/L (pH 5) for 24 h. Langmuir's and Freundlich's isotherm were used as adsorption models (Tab. 3). The collected data of

MPCA-700 agrees with the Langmuir adsorption model ( $R^2 = 0.9997$ ), suggesting the adsorption occurred in a monolayer formation. The calculated maximum adsorption capacity ( $q_m$ ) is 76.34 mg/g, comparable to those of other magnetic powdery porous adsorbents (Tab. 3).

### 3.3 Desorption Studies and Recyclability

To investigate the renewable recyclability of our monolith adsorbent, the desorption studies were performed using 0.001 HNO<sub>3</sub> as an eluent. The desorption conditions employed here are considered milder (pH 3) than those used in other works [28,30,36,37]. The desorption conditions employed in the present work showed no severe destruction of the porous structures and magnetic properties. Our desorption conditions were chosen based on the results of the pH effect on adsorption performance in Fig. 5A, associating to the reverse pH effect at pH 3 of materials. The decrease in adsorption capacity on the following adsorption-desorption cycles occurred since the incomplete removal of Pb<sup>2+</sup> ions on the MPCA-700. This resulted in some adsorption sites still being occupied by the adsorbed lead ions. When such adsorption sites were occupied, the number of available adsorption sites of the next cycle was then reduced.

Although %desorption of Pb<sup>2+</sup> ions in the first cycle was lower than 100% (Fig. 7), adsorption sites on the adsorbent were still available to host the Pb<sup>2+</sup> ions in the following cycles.

The %desorption remained steady after the third cycle, which probably resulted from pore filling effect of the adsorbent, and this has been generally observed in the adsorption of heavy metal and organic pollutants by carbonaceous materials [33,38,39]. From the results of the pH effect on adsorption performance (Fig. 5A) and the %desorption (Fig. 7), it can be claimed that the possible adsorption mechanism of Pb<sup>2+</sup> ions on the MPCA-700 involved both chemical and physical adsorption (pore filling effect) [33]. The interconnected micro/macroporous structures of MPCA-700 provided the acceptable reusability of MPCA-700 of 65.48% even after five cycles. This recyclability of the MPCA-700 can be comparable to other magnetic powder adsorbents (Tab. 3). Moreover, its magnetic properties and monolithic shape were still maintained. The reusability of this material through the mild regeneration conditions promisingly reduces the overall costs of the adsorption process. Furthermore, the stable monolithic feature makes MPCA-700 a candidate for the adsorption process in practical applications due to its easy operation, unlike the powdery adsorbents.

**Table 3:** Comparison of adsorption efficiency of Pb<sup>2+</sup> removal by magnetic carbon adsorbents prepared by different synthesis methods

Adsorbents	Methods	S <sub>BET</sub> [m <sup>2</sup> / g]	q <sub>m</sub> [mg/ g]	Conditions	k[g mg <sup>-1</sup> min <sup>-1</sup> ]	Magnetization [emu/g]	No. of recycles (eluent)	Ref.
Fe <sub>3</sub> O <sub>4</sub> NPs@AC@C <sub>4</sub> H <sub>8</sub> SO <sub>3</sub> H (powder)	Modified activated carbon	–	93.45	pH 5.5 T(K) 298 q <sub>0</sub> = 25 ppm Equilibrium time 10 min	6.0 × 10 <sup>-2</sup>	12	5 (0.1M HCl, pH 1)	[28]
Nanocarbon (powder)	Silica template	431	66.2	pH 6–7 T(K) 298	–	50.67	Not reported	[29]
FMBC (powder)	Pyrolysis and KMnO <sub>4</sub> activation	137	148	pH > 2.5–4 q <sub>0</sub> = 400 ppm Equilibrium time 600 min	3.67 × 10 <sup>-2</sup>	11.5	4 (1 M CH <sub>3</sub> COONa, pH 2.4)	[30]

Table 3 (continued).								
Adsorbents	Methods	$S_{\text{BET}}$ [m <sup>2</sup> / g]	$q_m$ [mg/ g]	Conditions	k[g mg <sup>-1</sup> min <sup>-1</sup> ]	Magnetization [emu/g]	No. of recycles (eluent)	Ref.
Oak powder/ Fe <sub>3</sub> O <sub>4</sub> (powder)	Precipitation	–	54.94	pH 6 T(K) 298 q <sub>0</sub> = 10 ppm Equilibrium time 50 min	$5.7 \times 10^{-2}$	38.45	Not reported	[31]
CCM 8000 (monolith)	Dip coating	469.8	71.95	pH 5 T(K) 303 q <sub>0</sub> = 250 ppm Equilibrium time 500 min	$10.18 \times 10^{-3}$	–	Not reported	[40]
<b>MPCA-700 (monolith)</b>	<b>Freeze- drying and pyrolysis</b>	<b>902</b>	<b>76.34</b>	<b>pH 5 T(K) 303 q<sub>0</sub> = 200 ppm Equilibrium time 200 min</b>	<b><math>3.07 \times 10^{-4}</math></b>	<b>8.8</b>	<b>5 (0.001 M HNO<sub>3</sub>, pH 3)</b>	<b>This work</b>

#### 4 Conclusion

The novel interconnected micro/macroporous structure of monolithic porous carbon adsorbent (MPCA) was achieved by using NaAlg and WBL as renewable precursors in an iron solution. The freeze-drying process generated the homogenous macroporous structure, and the subsequent pyrolysis process resulted in the interconnected micro/macroporous structure. MPCA-700 had high mechanical and magnetic stabilities. The high BET specific surface area and suitable micropore size (902 m<sup>2</sup>/g and 1.20 nm, respectively) of MPCA-700 significantly facilitated the adsorption performance towards Pb<sup>2+</sup> ions. The method of preparation of interconnected micro/macroporous structure of MPCA developed in this study tends to be further developed for large-scale production. The MPCA with magnetic properties can potentially be applied in the adsorption of other hazardous contaminations, as catalyst supports, and used in electrochemical storage devices.

**Acknowledgement:** We thank Development and Promotion of Science Technology Talents (DPST) Research Grant (Grant No. 017/2559) and the Institute for the Promotion of Teaching Science and Technology (IPST), Thailand for financial supports. Parichart Onsri was grateful to the Science Achievement Scholarship of Thailand (SAST) for allowance supports and the Department of Chemistry, Faculty of Science, Prince of Songkla University, Thailand, for supports with facilities. Partially financial support from the Center of Excellence for Innovation in Chemistry (PERCH-CIC), Ministry of Higher Education, Science, Research and Innovation is gratefully acknowledged. We thank Dr. Titilope John Jayeoye for English proof-reading.

**Funding Statement:** This work was funded by Development and Promotion of Science Technology Talents (DPST) Research Grant (Grant No. 017/2559) and the Institute for the Promotion of Teaching Science and Technology (IPST), Thailand.

**Conflicts of Interest:** The authors declare that they have no conflicts of interest to report regarding the present study.

## References

1. Jacob, J. M., Karthik, C., Saratale, R. G., Kumar, S. S., Prabakar, D. et al. (2018). Biological approaches to tackle heavy metal pollution. A survey of literature. *Journal of Environmental Management*, 217, 56–70. DOI 10.1016/j.jenvman.2018.03.077.
2. Nasaf, S. M., El-Nesr, E. M., Kamal, F. H., Badawy, N. A., Sherbiny, S. F. (2020). Gamma irradiation-induced preparation of gum arabic/poly (vinyl alcohol) copolymer hydrogels for removal of heavy metal ions from wastewater. *Arab Journal of Nuclear Sciences and Applications*, 53(1), 208–221.
3. Huang, Y., Li, S., Lin, H., Chen, J. (2014). Fabrication and characterization of mesoporous activated carbon from Lemna minor using one-step H<sub>3</sub>PO<sub>4</sub> activation for Pb(II) removal. *Applied Surface Science*, 317, 422–431. DOI 10.1016/j.apsusc.2014.08.152.
4. Omar, S., Muhamad, M. S., Chuan, L. T., Hadibarata, T., Teh, Z. C. (2019). A review on lead sources, occurrences, health effects, and treatment using hydroxyapatite (HAp) adsorbent made from fish waste. *Water Air and Soil Pollution*, 230(12), 21. DOI 10.1007/s11270-019-4312-9.
5. Askari, P., Faraji, A., Khayatian, G., Mohebbi, S. (2017). Effective ultrasound-assisted removal of heavy metal ions As(III), Hg(II), and Pb(II) from aqueous solution by new MgO/CuO and MgO/MnO<sub>2</sub> nanocomposites. *Journal of the Iranian Chemical Society*, 14(3), 613–621. DOI 10.1007/s13738-016-1011-y.
6. Chen, L. M., Yu, H. Y., Deutschman, C., Yang, T., Tam, K. C. (2020). Novel design of Fe-Cu alloy coated cellulose nanocrystals with strong antibacterial ability and efficient Pb<sup>2+</sup> removal. *Carbohydrate Polymers*, 234, 8.
7. Purnendu, Satapathi S. (2017). Graphene-based 3D xerogel as adsorbent for removal of heavy metal ions from industrial wastewater. *Journal of Renewable Materials*, 5(2), 96–102. DOI 10.7569/JRM.2016.634134.
8. Du, Q., Li, G. X., Zhang, S. S., Song, J. P., Zhao, Y. et al. (2020). High-dispersion zero-valent iron particles stabilized by artificial humic acid for lead ion removal. *Journal of Hazardous Materials*, 383, 9. DOI 10.1016/j.jhazmat.2019.121170.
9. Deng, S., Liu, X. H., Liao, J. B., Lin, H., Liu, F. (2019). PEI modified multiwalled carbon nanotube as a novel additive in PAN nanofiber membrane for enhanced removal of heavy metal ions. *Chemical Engineering Journal*, 375, 11. DOI 10.1016/j.cej.2019.122086.
10. Thaci, B. S., Gashi, S. T. (2019). Reverse osmosis removal of heavy metals from wastewater effluents using biowaste materials pretreatment. *Polish Journal of Environmental Studies*, 28(1), 337–341. DOI 10.15244/pjoes/81268.
11. Kudo, Y., Nakamori, T., Numako, C. (2018). Pb(II) extraction with benzo-18-crown-6 ether into benzene under the co-presence of Cd(II) nitrate in water. *Inorganics*, 6(3), 16. DOI 10.3390/inorganics6030077.
12. Wang, G. H., Fan, W. Z., Li, Q., Deng, N. S. (2019). Enhanced photocatalytic new coccine degradation and Pb(II) reduction over graphene oxide-TiO<sub>2</sub> composite in the presence of aspartic acid-beta-cyclodextrin. *Chemosphere*, 216, 707–714. DOI 10.1016/j.chemosphere.2018.10.199.
13. Teng, Z. D., Shao, W., Zhang, K. Y., Yu, F. L., Huo, Y. Q. et al. (2020). Enhanced passivation of lead with immobilized phosphate solubilizing bacteria beads loaded with biochar/ nanoscale zero valent iron composite. *Journal of Hazardous Materials*, 384, 11. DOI 10.1016/j.jhazmat.2019.121505.
14. Zhao, X. R., Xu, X., Teng, J., Zhou, N., Zhou, Z. et al. (2019). Three-dimensional porous graphene oxide-maize amylopectin composites with controllable pore-sizes and good adsorption-desorption properties: Facile fabrication and reutilization, and the adsorption mechanism. *Ecotoxicology and Environmental Safety*, 176, 11–19. DOI 10.1016/j.ecoenv.2019.03.069.
15. Rattanachueskul, N., Saning, A., Kaowphong, S., Chumha, N., Chuenchom, L. (2017). Magnetic carbon composites with a hierarchical structure for adsorption of tetracycline, prepared from sugarcane bagasse via hydrothermal carbonization coupled with simple heat treatment process. *Bioresource Technology*, 226, 164–172. DOI 10.1016/j.biortech.2016.12.024.
16. Feng, Y., Liu, P., Wang, Y. X., Finfrock, Y. Z., Xie, X. J. et al. (2020). Distribution and speciation of iron in Fe-modified biochars and its application in removal of As(V), As(III), Cr(VI), and Hg(II): An X-ray absorption study. *Journal of Hazardous Materials*, 384, 10. DOI 10.1016/j.jhazmat.2019.121342.

17. Joshi, S., Sharma, M., Kumari, A., Shrestha, S., Shrestha, B. (2019). Arsenic removal from water by adsorption onto iron oxide/nano-porous carbon magnetic composite. *Applied Sciences-Basel*, 9(18), 12.
18. Chen, X. Y., Zhu, J. (2019). Alginate composite hydrogel bead with multilayer flake structure for dye adsorptions. *Journal of Renewable Materials*, 7(10), 983–996. DOI 10.32604/jrm.2019.07325.
19. Hong, H. J., Kim, B. G., Ryu, J., Park, I. S., Chung, K. S. et al. (2018). Preparation of highly stable zeolite-alginate foam composite for strontium (Sr-90) removal from seawater and evaluation of Sr adsorption performance. *Journal of Environmental Management*, 205, 192–200. DOI 10.1016/j.jenvman.2017.09.072.
20. Babel, K., Jurewicz, K. (2008). KOH activated lignin based nanostructured carbon exhibiting high hydrogen electrosorption. *Carbon*, 46(14), 1948–1956. DOI 10.1016/j.carbon.2008.08.005.
21. Torres, L. A. Z., Woiciechowski, A. L., Tanobe, V. O. D., Karp, S. G., Lorenci, L. C. G. et al. (2020). Lignin as a potential source of high-added value compounds: A review. *Journal of Cleaner Production*, 263, 18.
22. Zeng, Z. H., Ma, X. Y. D., Zhang, Y. F., Wang, Z., Ng, B. F. et al. (2019). Robust lignin-based aerogel filters: High-efficiency capture of ultrafine airborne particulates and the mechanism. *ACS Sustainable Chemistry & Engineering*, 7(7), 6959–6968. DOI 10.1021/acssuschemeng.8b06567.
23. Saning, A., Herou, S., Dechtrirat, D., Ieosakulrat, C., Pakawatpanurut, P. et al. (2019). Green and sustainable zero-waste conversion of water hyacinth (*Eichhornia crassipes*) into superior magnetic carbon composite adsorbents and supercapacitor electrodes. *RSC Advances*, 9(42), 24248–24258. DOI 10.1039/C9RA03873F.
24. ElKhatat, A. M., Al-Muhtaseb, S. A. (2011). Advances in tailoring resorcinol-formaldehyde organic and carbon gels. *Advanced Materials*, 23(26), 2887–2903. DOI 10.1002/adma.201100283.
25. Tamon, H., Ishizaka, H., Yamamoto, T., Suzuki, T. (2000). Influence of freeze-drying conditions on the mesoporosity of organic gels as carbon precursors. *Carbon*, 38(7), 1099–1105. DOI 10.1016/S0008-6223(99)00235-3.
26. Cho, M. J., Karaaslan, M., Wang, H., Rennecker, S. (2018). Greener transformation of lignin into ultralight multifunctional materials. *Journal of Materials Chemistry A*, 6(42), 20973–20981. DOI 10.1039/C8TA07802E.
27. Mahawong, S., Dechtrirat, D., Watcharin, W., Wattanasin, P., Muensit, N. et al. (2020). Mesoporous magnetic carbon adsorbents prepared from sugarcane bagasse and Fe<sup>2+</sup> and Fe<sup>3+</sup> via simultaneous magnetization and activation for tetracycline adsorption. *Science of Advanced Materials*, 12(2), 161–172. DOI 10.1166/sam.2020.3621.
28. Nejadshafiee, V., Islami, M. R. (2019). Adsorption capacity of heavy metal ions using sultone-modified magnetic activated carbon as a bio-adsorbent. *Materials Science & Engineering C-Materials for Biological Applications*, 101, 42–52. DOI 10.1016/j.msec.2019.03.081.
29. Guo, K., Larson, S. L., Ballard, J. H., Arslan, Z., Zhang, R. et al. (2018). Novel magnetic nanocarbon and its adsorption of Hg and Pb from water. *Water Air and Soil Pollution*, 229(4), 9. DOI 10.1007/s11270-018-3770-9.
30. Sun, C., Chen, T., Huang, Q. X., Wang, J., Lu, S. Y. et al. (2019). Enhanced adsorption for Pb(II) and Cd(II) of magnetic rice husk biochar by KMnO<sub>4</sub> modification. *Environmental Science and Pollution Research*, 26(9), 8902–8913. DOI 10.1007/s11356-019-04321-z.
31. Shafiee, M., Foroutan, R., Fouladi, K., Ahmadlouydarab, M., Ramavandi, B. et al. (2019). Application of oak powder/Fe<sub>3</sub>O<sub>4</sub> magnetic composite in toxic metals removal from aqueous solutions. *Advanced Powder Technology*, 30(3), 544–554. DOI 10.1016/j.apt.2018.12.006.
32. Li, Z., Ge, Y., Wan, L. (2015). Fabrication of a green porous lignin-based sphere for the removal of lead ions from aqueous media. *Journal of Hazardous Materials*, 285, 77–83. DOI 10.1016/j.jhazmat.2014.11.033.
33. Deng, R., Huang, D. L., Zeng, G. M., Wan, J., Xue, W. J. et al. (2019). Decontamination of lead and tetracycline from aqueous solution by a promising carbonaceous nanocomposite: Interaction and mechanisms insight. *Bioresource Technology*, 283, 277–285. DOI 10.1016/j.biortech.2019.03.086.
34. Liu, Z. X., Zhou, X. T., Liu, C. J. (2019). N-doped porous carbon material prepared via direct ink writing for the removal of methylene blue. *Diamond and Related Materials*, 95, 121–126. DOI 10.1016/j.diamond.2019.04.010.
35. Zhang, W. L., Li, H. H., Tang, J. M., Lu, H. J., Liu, Y. Q. (2019). Ginger straw waste-derived porous carbons as effective adsorbents toward methylene blue. *Molecules*, 24(3), 8.

36. Ayyappan, R., Sophia, A. C., Swaminathan, K., Sandhya, S. (2005). Removal of Pb(II) from aqueous solution using carbon derived from agricultural wastes. *Process Biochemistry*, 40(3–4), 1293–1299. DOI 10.1016/j.procbio.2004.05.007.
37. Yang, B., Wei, Y., Liu, Q., Luo, Y., Qiu, S. et al. (2019). Polyvinylpyrrolidone functionalized magnetic graphene-based composites for highly efficient removal of lead from wastewater. *Colloids and Surfaces A: Physicochemical and Engineering Aspects*, 582, 123927. DOI 10.1016/j.colsurfa.2019.123927.
38. Wang, H., Fang, C. R., Wang, Q., Chu, Y. X., Song, Y. L. et al. (2018). Sorption of tetracycline on biochar derived from rice straw and swine manure. *RSC Advances*, 8(29), 16260–16268. DOI 10.1039/C8RA01454J.
39. Huang, D. L., Wang, X., Zhang, C., Zeng, G. M., Peng, Z. W. et al. (2017). Sorptive removal of ionizable antibiotic sulfamethazine from aqueous solution by graphene oxide-coated biochar nanocomposites: Influencing factors and mechanism. *Chemosphere*, 186, 414–421. DOI 10.1016/j.chemosphere.2017.07.154.
40. Teoh, Y. P., Khan, M. A., Choong, T. S. Y. (2013). Kinetic and isotherm studies for lead adsorption from aqueous phase on carbon coated monolith. *Chemical Engineering Journal*, 217, 248–255. DOI 10.1016/j.cej.2012.12.013.